

Deep Learning Applied to Beamforming in Synthetic Aperture Ultrasound

Nissim Peretz, and Arie Feuer, *Life Fellow, IEEE*

Abstract—Deep learning methods can be found in many medical imaging applications. Recently, those methods were applied directly to the RF ultrasound multi-channel data to enhance the quality of the reconstructed images. In this paper, we apply a deep neural network to medical ultrasound imaging in the beamforming stage. Specifically, we train the network using simulated multi-channel data from two arrays with different sizes, using a variety of direction of arrival (DOA) angles, and test its generalization performance on real cardiac data. We demonstrate that our method can be used to improve image quality over standard methods, both in terms of resolution and contrast. Alternatively, it can be used to reduce the number of elements in the array, while maintaining the image quality. The utility of our method is demonstrated on both simulated and real data.

Index Terms—Beamforming, Multichannel Signal Enhancement, Deep learning, Synthetic Aperture Ultrasound.

I. INTRODUCTION

BEAMFORMING is a crucial task in a variety of fields including, radar, sonar, acoustics and wireless communication [1]. While there are several different approaches in the literature, the Delay-And-Sum (DAS) beamforming is the most common method in medical ultrasound imaging. An image is formed by transmitting a narrow beam in several scanning angles, and dynamically delaying and summing the received signals from all channels. The images produced by DAS are typically degraded by sidelobes artifacts, resulting from the processing applied on the data collected. Sidelobes are considered as interferences that mask the desired signal, reducing the contrast-to-noise ratio (CNR). The sidelobe level of the DAS beamformer can be controlled using *aperture apodization* (amplitude weighting of the elements across the aperture), resulting in increased contrast at the expense of resolution. Thus, the weights used in the beamforming process are designed to trade off sidelobes reduction for lateral resolution.

The conventional ultrasound scanning method transmits pulses in one direction at a time. The signals received by the transducer, are used to reconstruct a part of an image corresponding to the scan line. This set of lines is then interpolated onto a Cartesian grid, and a single frame can be created. The process is repeated sequentially to create the next frames. Consequently, the acquisition time is limited by the speed of sound. Another limiting factor in conventional

ultrasound imaging is the single transmit focus, where the transmit beam is only focused at one depth. This can be solved by image compounding [2] using several beams with different transmit focus, resulting in a very large depth of focus, but the frame rate is then correspondingly decreased. Therefore, there is much interest in searching alternatives to the conventional methods, where the single transmit focusing and frame rate constraints can be alleviated. An alternative is to use *Synthetic Aperture* imaging techniques.

In the first technique, known as *Synthetic Aperture* (SA) ultrasound [3], only a single array element transmits and receives each time. All array elements transmit/receive sequentially one at a time and the received echoes are sampled and stored. SA increases the frame rate, but the main limitation of the technique is the low SNR and poor contrast resolution (see [3]).

In the second technique, known as *Synthetic Transmit Aperture* (STA) ultrasound [4], a single element transmits and all elements receive the reflected signals simultaneously. The SNR is increased compared to SA, since the image reconstruction uses a larger amount of data collected by all elements. This multistatic approach produces the image in a tomographic manner in which the numerous transmit/receive angles improve the resolution and contrast of the reconstructed image. The main limitation of the STA technique is the very large amount of data that needs to be stored in memory.

Norton [5] has modeled the SA method, under some simplifying assumptions, the process of generating the data from an imaged object as a forward mapping. Hence, generating the (unknown) image from the accumulated data is viewed as an inverse mapping. He proceeded to analytically generate a closed form expression for this inverse mapping.

When the data is fed into the inverse system, it is convolved with the appropriate impulse response to produce the imaged object. DAS beamforming is a linear approximate solution to the inverse system, which is not accurate in the presence of multiple reflections and multiple varying acoustic properties.

In recent years, the field of Deep Learning has gained a lot of momentum in solving such inverse problems in imaging [6]. Inspired by the feasibility and success of this field, we propose in this work to replace the traditional DAS beamforming process with an alternative using DNN as part of the scanned image forming.

A. Related Work

A variety of ultrasound reconstruction approaches utilizing deep learning have been proposed in the literature.

N. Peretz is with the Department of Electrical Engineering, Technion-Israel Institute of Technology, Haifa 3200003, Israel (e-mail: nis-simp@campus.technion.ac.il).

A. Feuer is with the Department of Electrical Engineering, Technion-Israel Institute of Technology, Haifa 3200003, Israel (e-mail: feuer@ee.technion.ac.il).

Luchies and Byram [7] investigated the use of multiple networks for reducing off-axis single point scattering in ultrasound images, processing the data in the frequency domain using the short-time Fourier transform. For each frequency bin, the array samples are processed by a different network. The data was transformed back into the time domain using the inverse Fourier-transform and summed across the array to create a signal that corresponds to a single depth of channel data. In [8], the authors aim to extend their previous work, by training multiple networks using multiple point target reflections instead of single point target reflection.

Gasse et al. [9] proposed to exploit neural networks to reduce the number of emitted transmissions in coherent plane-wave compounding. A convolutional neural network (CNN) was trained to reconstruct high-quality images, based on a small number of transmissions. The authors in [10] posed the beamforming process in ultrasound as a segmentation problem and applied a CNN to segment cyst phantoms.

In [11], [12], the authors suggested exploiting CNNs to reconstruct high-quality images acquired through high-frame rate ultrasound techniques, such as multi-line acquisition (MLA) and multi-line transmission (MLT). They propose to train a network that takes MLA/MLT channel data as an input, and reconstructs images such that it mimics the operation of a single-line acquisition (SLA). In [13], they proposed to learn the parameters of the forward model simultaneously with the image reconstruction process, that is, to jointly learn the end-to-end transmit and receive beamformers.

In [14], the authors proposed a method to reconstruct high-quality ultrasound images in real-time on sub-sampled scan lines data. The network learns a mapping from a sub-sampled collection of scan lines to high-quality images, which were generated offline with a minimum variance beamforming technique.

Luijten et al. [15] proposed to approximate the time-consuming Eigen Based Minimum Variance beamformer using a CNN, which enable a real-time implementation of adaptive beamforming in plane-wave imaging. In [16], the authors proposed to use a CNN to learn a non-linear mapping from the low-quality images, reconstructed from a single plane-wave, to the high-quality images, reconstructed from multiple plane-waves.

Reviewing all the mentioned works, it appears that none of the results relates to the aperture size and number sensors in the probe which is one of the main attributes of our work. Furthermore, the Synthetic Aperture imaging techniques are not addressed. Concluding this review, it appears that the potential benefits of applying deep learning in ultrasound medical imaging are yet to be exhausted.

B. Contributions

The image reconstruction method we present here, DNN Beamforming (DNNB), combines two independent novel ideas. One, that a DNN can be trained to use scanning data generated by a given array size to emulate scanning data from a larger array, and two, that a DNN can be trained to suppress sidelobe artifacts when applied with DAS. While

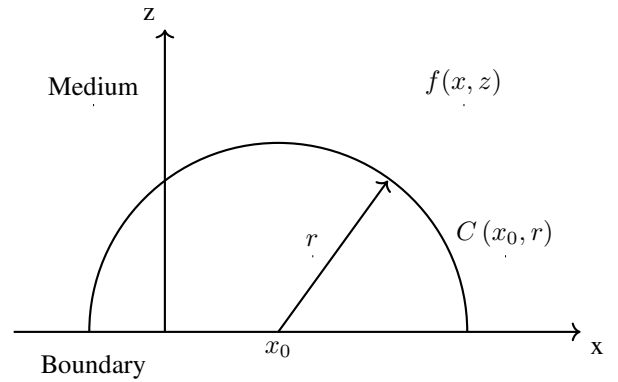


Fig. 1: SA technique: circular wave front transmitted from x_0 , and received at x_0 .

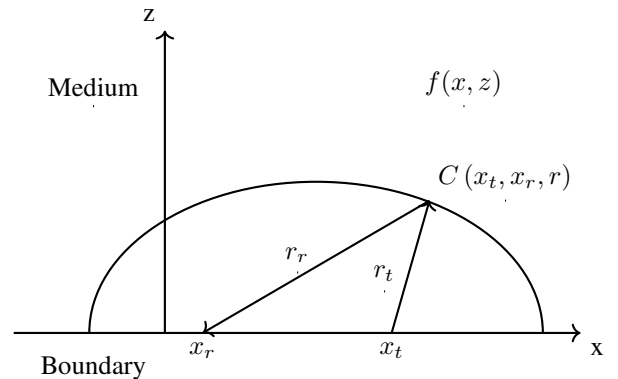


Fig. 2: STA technique: circular wave front transmitted from x_t , and received at x_r .

initially we have trained two DNNs to achieve the above, by using synthetic data for the network training, we managed to combine the two into a single network. The experiments we present here are all using a single DNN trained for both tasks.

We applied our method, DNNB, on three major scanning techniques: *Synthetic Aperture (SA)*, *Synthetic Transmit Aperture (STA)* and conventional *Phased Array (PA)*, using a properly trained neural network as part of the beamforming process in each. We demonstrate that our method clearly outperforms the DAS approach for all three techniques in terms of the resulting image quality. The resulting images are almost free of DAS induced sidelobe artifacts and have significantly improved lateral resolution compared to DAS images using the *same aperture*.

We visualize three potential scenarios for applying our method. One, improving the reconstructed image quality of a given scanning array size. Two, using a smaller scanner, which is frequently desirable, while maintaining an acceptable reconstructed image quality, and three, when data size is an issue with a given size scanner, using full array size in transmission and downsampling the received data - using only the data from a subset or receiving elements.

II. SIGNAL MODEL

A. Synthetic Aperture Beamforming

The full mathematical background for using the SA technique is given in [5], and a summary is provided here for the

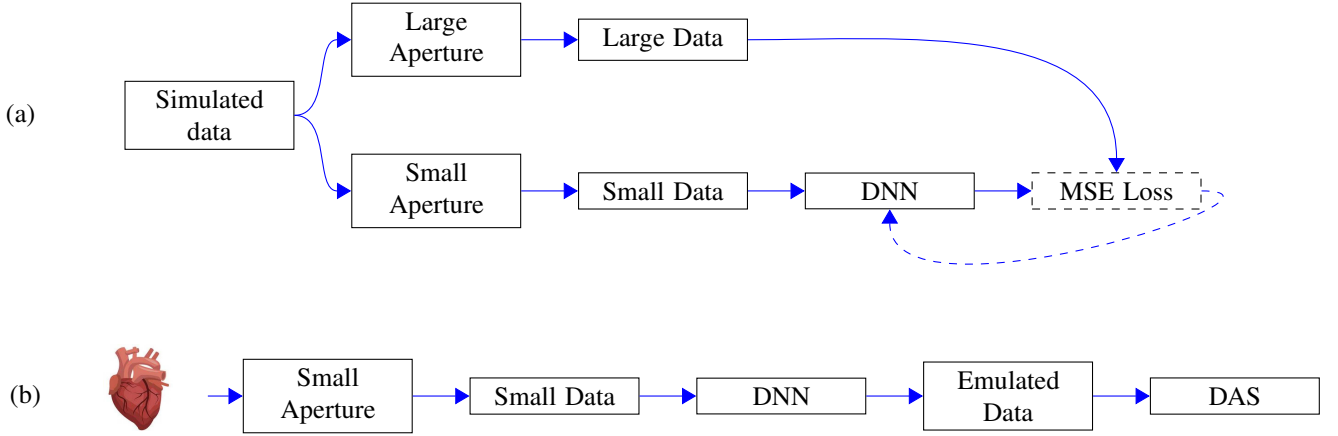


Fig. 3: The setup for the two stages of our method: (a) The network training. (b) The network utilization.

benefit of the reader.

We consider a two-dimensional reflecting medium, denoted by $f(x, z)$ in the $x-z$ plane and the omnidirectional transducer located at x_0 on the boundary (see Figure 1). Suppose a narrow pulse is transmitted by the transducer, propagates isotropically in the $x-z$ plane. Following the transmission of that pulse, the transducer is switched to a receiving mode and the returning reflections are recorded as a function of time. Let $\mathcal{C}(x_0, r)$ denote the semicircular path of radius r and center at $(x = x_0, z = 0)$. After a further delay of r/c (where c is the speed of sound), the returned pulses originating from points lying along this path, arrive simultaneously at the receiver and are integrated there. The transducer is then shifted to a new location on the x axis and the acquisition process is repeated. This way, we generate the two-dimensional (data) function $g(x_0, r)$, where the connection between $f(x, z)$ and $g(x_0, r)$ is given by

$$\begin{aligned} g_{SA}(x_0, r) &= \oint_{\mathcal{C}(x_0, r)} f(x, z) dl \\ &= \int_{-\infty}^{\infty} \int_{-\infty}^{\infty} f(x, z) \delta \left(r - \left[z^2 + (x_0 - x)^2 \right]^{\frac{1}{2}} \right) dx dz \end{aligned} \quad (1)$$

which denotes the line integral of $f(x, z)$ along the semicircular path $\mathcal{C}(x_0, r)$. Note that the transmitted signal is assumed to be the Dirac Delta. The goal is to express the original function $f(x, z)$ in terms of $g(x_0, r)$. Norton managed to derive an analytic expression for this in a form of *deconvolution*. We will further discuss some aspects of his work in the sequel.

Clearly, a more efficient utilization of an array could be achieved by transmitting from one element and receiving with all transducers. This is the STA technique, presented next.

B. Synthetic Transmit Aperture Beamforming

A generalization of the SA technique is the Synthetic Transmit Aperture (STA) [3]. Similar to SA, a single element is used in transmission, whereas in receive, all elements are used and a low-resolution image can be formed. After the first element is used to create the first low-resolution image, the successive element transmits to create another low-resolution image. Once all the elements are used in transmission, the

low-resolution images are compounded to form the final high-resolution image. As opposed to SA, STA imaging has the advantage of lower sidelobe level and a higher SNR ratio. The data generation process can now be modeled by

$$\begin{aligned} g_{STA}(x_t, x_r, r) &= \oint_{\mathcal{C}(x_t, x_r, r)} f(x, z) dl \\ &= \int_{-\infty}^{\infty} \int_{-\infty}^{\infty} f(x, z) \delta \left(r - \frac{1}{2} \left(\left[z^2 + (x_t - x)^2 \right]^{\frac{1}{2}} \right. \right. \\ &\quad \left. \left. + \left[z^2 + (x_r - x)^2 \right]^{\frac{1}{2}} \right) \right) dx dz \end{aligned} \quad (2)$$

where x_t and x_r are the locations of transmitting and receiving elements respectively, and $r (= t/c)$ represents the time passed from transmission. In this case, we note that the recorded data is the result of integration of reflected signal from points (x, z) along the line $\mathcal{C}(x_t, x_r, r)$ which is half an ellipse with focal points at x_t, x_r and r is the sum of distances to these two focal points (see Figure 2). The result is a three dimensional data function, $g(x_t, x_r, r)$. This model is clearly more complex than the SA case and to our knowledge no analytical result for the reconstruction, similar to the one for the SA case, is available. However, we wish to point out that since clearly, $g_{SA}(x_0, r) = g_{STA}(x_0, x_0, \frac{r}{2})$, the exact reconstruction of the image from data in the STA case should be possible as well.

C. Conventional Phased Array Beamforming

Whereas in SA/STA techniques only a single element is active during the transmission phase, in conventional Phased Array imaging all array elements are used during both transmit and receive. By using all the elements simultaneously at the transmit phase, a beam is created and electronically swept over the region of interest (ROI) in the image.

III. DEEP LEARNING BASED BEAMFORMING

As mentioned earlier, in his work, [5] and [17], Norton derived an analytical inverse mapping of Eqn. (1). He further derived an analytic expression for the result of applying the DAS operation on the SA generated data. While his analysis

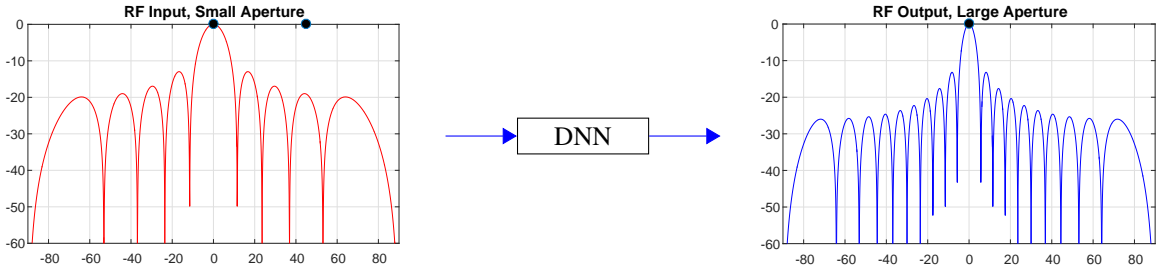


Fig. 4: An illustration of the proposed training method. Left: receive beam-pattern of the small aperture (red). Right: receive beam-pattern of the large aperture (blue). Black dots represent point targets.

was based on the assumption of an infinite array, in [17] we find an analysis and discussion of how having a finite array affects the image reconstruction results both for the deconvolution and the DAS methods. The observations made by Norton provided the motivation for our work. Specifically:

- 1) The reconstruction using DAS is only an attempt to approximate the exact reconstruction, the deconvolution. Namely, since both use the same data, the DAS does *not fully utilize the data collected by the array*.
- 2) Constrained to a finite size array deteriorates the quality of the reconstructed image whether using the deconvolution or the DAS. The smaller the array, the worse the reconstructed image quality. However, *the impact on the DAS result is more significant*.

With these two observations and inspired by [18] who applied deep learning to get super resolution from a single image, we have developed the method we present here. Given data from a finite size aperture scan of an image, we train a neural network to emulate data resulting from scanning the same image with a *larger aperture*. Then, applying DAS on the larger (emulated) data we generate a considerably improved reconstructed image. This result is directly related to a fundamental result in array signal processing: Increasing array size while keeping the same inter-element spacing, achieves a narrower main lobe (better lateral resolution), and lower sidelobes (better contrast) relative to a small array size.

In Figure 3 we present the setup for the two stages of our method: The network training and the network utilization.

In our experiments with neural networks, we managed to achieve a further improvement of contrast resolution using a neural network trained to reduce sidelobes. To this end, in addition to its emulation role, we also train the network to place deeper nulls in the sidelobes locations. To achieve this, the input training example contains a multichannel waveform as received from two targets: one in the main lobe and another in a random sidelobe. The output training example contains a multichannel waveform as received from just a single target in the main lobe. An illustration of this proposed training process is given in Figure 4.

We draw some similarity to our problem from [7], who trained a network to suppress off-axis scattering outside the first nulls of the beam. However, there are significant differences between our approaches. First, [7] operates in the frequency domain via the short-time Fourier transform, where different networks were trained for different frequencies. We

propose to operate in the space/time domain, training a single network. Second, we use two separate arrays of different sizes for the data generation stage, whereas [7] uses a single array whose size is fixed. Finally, as pointed out earlier, we are also aiming at providing an improvement in lateral resolution of the reconstructed image.

IV. EXPERIMENTS

The experiments we describe in the sequel are divided into two parts. In the first we used simulated data while in the second we used real cardiac data. In both parts, we compare the image quality for a given (small) array, using DAS and the DNNB. Our method clearly results in significantly superior image quality. An interesting question is how close is the data emulated by the DNN to real data generated by the large array. Using simulated data, we could also compare the performance of our trained DNN with DAS applied to data generated by the large array. This can be observed in Table II and Figure 5.

We also wish to point out that with the real data experiments, we were constrained by the available data. So, since all this data was collected by a given array, both transmit and receive, we experimented only with the possibility of a small array in receive where small array simply means using the data from a subset of receiving elements.

A. Training The Network

Training the network in a supervised manner requires a training data set with a large number of low/high-resolution multichannel waveform pairs. Due to practical constraints, we used in our experiments for the training stage of the DNN only data simulated by FIELD II [19]. The data set comprised pairs of 30,000 point targets randomly positioned in various DOA angles, simulated by a uniform linear array of 33 elements (low-resolution signals), and the corresponding point targets simulated by a uniform linear array of 65 elements (high-resolution signal). We note that our choice of the ratio $65/33 \approx 2$ seems quite arbitrary but in our experiments seemed to produce good results.

The synthetic data generation enabled us to train simultaneously the network for both the emulation part and the sidelobe suppression part as explained earlier. Given a set of high-resolution multichannel waveform matrices, and their corresponding low-resolution multichannel waveform matrices, we train the network to minimize the mean-squared error (MSE) loss function (see Figure 3).

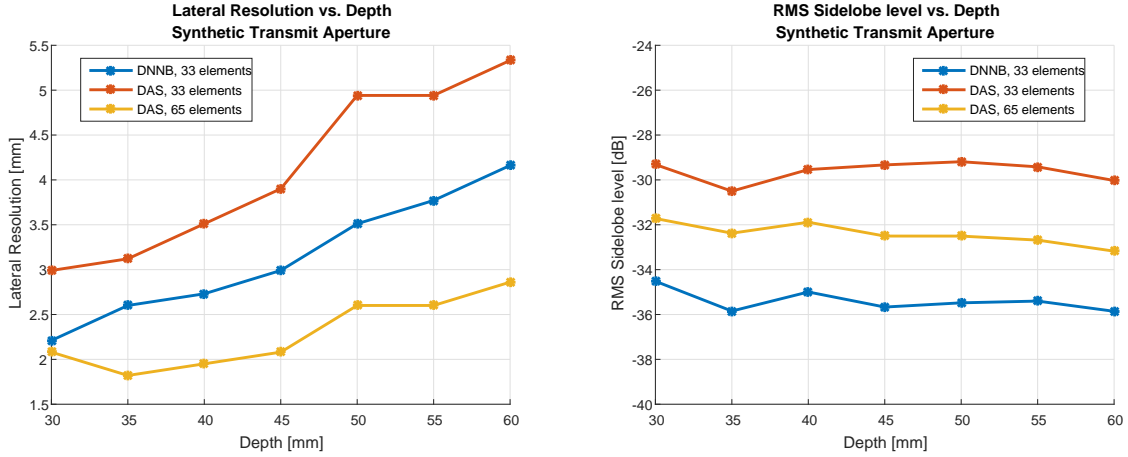


Fig. 5: Left: STA lateral resolution vs. depth. Right: STA RMS sidelobe level vs. depth.

TABLE I: Field II simulation parameters

Parameter	Value
c (Speed of Sound)	1540 [m/sec]
f_0 (Central Frequency)	3.5 [MHz]
f_s (Sampling Frequency)	16 [MHz]
Element Width	0.220 [mm]
Element Height	5 [mm]
Kerf	0.044 [mm]
Number of Elements	33/65
Apodization	None
Number of Scan Lines	65
Sector Size	48°
Tx Focus	50 [mm]

Clearly, for each of the scanning techniques we experimented with, SA, STA and PA, a separate DNN had to be trained. In the conventional PA method, all scan lines typically have a fixed origin on the transducer surface, but are steered in a fan pattern to create the image. We delay each channel in the training data set to focus at a point in the image, which is the only pre-processing we perform on the data before being fed into the DNN.

Architecture: We used a fully connected neural network, followed by convolutional layers. The number of hidden layers was 6. The Leaky Rectified Linear Unit (LeakyReLU) was chosen as the activation function of hidden layers, where the last layer was linear. The full network effectively scales the input multichannel waveform dimensions up by a factor 2. We used Keras API [20] on top of a TensorFlow [21] backend written in Python to create and train the network.

Optimization: The network was trained for 50 epochs using the Adam optimizer [22] with a learning rate of 10^{-3} , and learning rate decay of 10^{-8} . As mentioned earlier, we used the MSE as the loss function. We reduced the learning rate by a factor of 2 when the validation loss has stopped improving. Weights of all neurons in the network were initialized using the Uniform distribution. The mini-batch size was chosen to be 64 samples to attain a good trade-off between the efficiency of not having all training data in memory, and model convergence speed.

B. Simulation Setup

To evaluate our proposed beamformer, we first tested it on synthetic cyst phantom, and then on a set of consecutive frames of cardiac ultrasound data. The cyst phantom scan was done using an aperture comprising 33/65 transducer elements, operating with a central frequency of $f_0 = 3.5$ [MHz]. The width of each element, measured along the \hat{x} axis, was $\frac{1}{2}\lambda = \frac{c}{2f_0} = 0.220$ [mm], and the height, measured along the \hat{y} axis, was 5 [mm]. The elements were arranged along the \hat{x} axis, with a 0.044 [mm] inter-element spacing (kerf). The transmitted pulse was simulated by exciting each element with 1.75 periods of a sinusoid of frequency f_0 , where the delays were adjusted such that the transmission focal point was at depth $r = 50$ [mm]. No apodization was applied on transmission (rectangular window).

The RF signals of each channel were sampled at 16 [MHz]. During the simulations, a 48° sector was imaged using 65 scan lines. The envelope was extracted using the Hilbert transform, and the appropriate beamforming was applied according to the selected technique. The simulation parameter settings are summarized in Table I.

C. Quality Measures

In this section, we describe the quantitative measurements used to assess the proposed method, DNNB, performance in terms of lateral resolution and sidelobes level. The lateral resolution is evaluated by computing the full width at half maximum of the point spread function in the lateral axis. A quantitative measure of contrast can be calculated by the contrast-to-noise ratio (CNR) and contrast ratio (CR):

$$\text{CNR} = \frac{|\mu_b - \mu_c|}{\sqrt{\sigma_b^2 + \sigma_c^2}}$$

$$\text{CR} = 20 \log_{10} \left(\frac{\mu_c}{\mu_b} \right)$$

where μ_c and μ_b are the mean image intensities, respectively in a region inside the phantom cyst or in the surrounding background, and σ_c^2 , σ_b^2 are the corresponding variances [23]. A quantitative measure of sidelobes level is the root mean square

(RMS) sidelobes level, which is evaluated by computing the intensity of the point spread function outside the mainlobe.

V. RESULTS

A. Simulated Data

Next, we present the results of our experiments obtained by applying DNNB to ultrasound signals simulated using the Field II program for an image of cyst phantom.

1) *SA Results:* As can be seen in Figure 6, the main effect of the DNNB is in the reduction of the lateral sidelobes, which is expressed in contrast enhancement: the CR is -5.7779 [dB] compared to -3.0151 [dB] with DAS 33 elements. The CNR is also improved, 0.0296 , compared to 0.0165 with DAS 33 elements. In addition, it can be seen in Figure 6 that DNNB provides better sidelobe interference reduction within the cyst, while preserving the speckle texture in the region outside the cyst. This provides empirical justification for the proposed training method, where we trained the network to place deeper nulls at the sidelobes.

2) *STA Results:* We next compare the results of a cyst phantom, obtained by Synthetic Transmit Aperture imaging (see Figure 7). The contrast of the anechoic cyst is improved when applying DNNB: the CR is -7.4324 [dB] compared to -4.9211 [dB] with DAS 33 elements. The CNR is also improved: 0.0362 , compared to 0.0259 with DAS 33 elements. We also study the robustness of DNNB to depth changes. To that end, point targets were placed at various depths. A graph of STA performance as a function of depth is presented in Figure 5.

3) *Conventional Phased Array imaging Results:* We next proceed to the results of a cyst phantom obtained by Conventional Phased Array (PA) imaging. The image produced by DNNB is characterized by a very sharp transition from speckle to cyst region, noted in Figure 8. As expected, the contrast of the anechoic cyst is improved when applying DNNB: the CR is -10.8735 [dB] while it is -5.2532 [dB] with DAS 33 elements. The CNR is also improved: 0.0591 , while it is 0.0343 with DAS 33 elements.

The resulting values of lateral resolution and RMS sidelobe level of a single point target are summarized in Table II. It can be noted that DNNB 33 elements provide a prominent improvement in lateral resolution and sidelobes level compared to standard DAS 33 elements processing.

B. Cardiac Data Experiments

We applied the DNNB on real cardiac ultrasound data. This allows for a (partial) qualitative assessment of the proposed technique. The acquisition was performed using a wideband phased array ultrasound scanner consist of 64 elements. Operating in second harmonic imaging mode, pulses were transmitted at 1.7 [MHz], and the corresponding second harmonic signal, centered at 3.42 [MHz], was then acquired. Data from all acquisition channels were sampled at 20 [MHz] and collected along 120 beams, forming a 75° sector. The beamforming results obtained for the cardiac data are depicted in Figure 10.

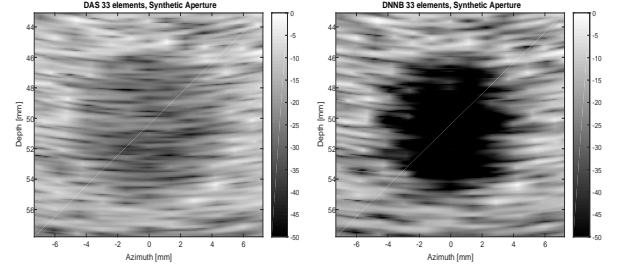


Fig. 6: SA results of standard DAS and the proposed DNN for phantom data, using an array of 33 elements.

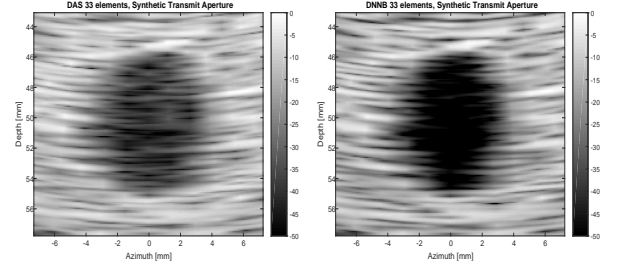


Fig. 7: STA results of standard DAS and the proposed DNN for phantom data, using an array of 33 elements.

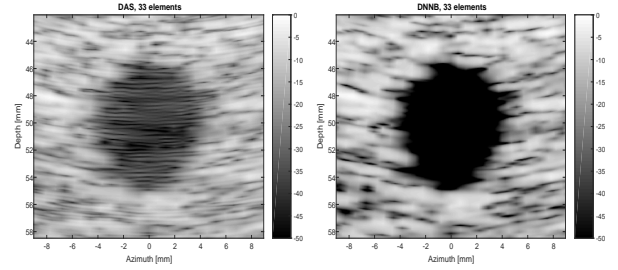


Fig. 8: PA results of standard DAS and the proposed DNN for phantom data, using an array of 33 elements.

TABLE II: SA, STA and Phased Array results for lateral resolution and RMS sidelobe level.

Method	Lateral Resolution [mm]	RMS sidelobe level [dB]
SA DAS 65 elements	1.951	-30.95
SA DAS 33 elements	3.961	-27.71
SA DNNB 33 elements	2.341	-32.34
STA DAS 65 elements	2.601	-32.51
STA DAS 33 elements	4.871	-29.19
STA DNNB 33 elements	3.511	-35.48
PA DAS 65 elements	2.812	-36.23
PA DAS 33 elements	4.941	-31.76
PA DNNB 33 elements	3.774	-39.12

C. Cardiac Data Experiments - Receive Aperture Reduction

We used *in-vivo* acquisitions from [24] to study the robustness of the proposed beamformer to different aperture sizes, where the receive aperture was reduced by a factor of 2, 4, and 8. The results are illustrated in Figure 11a, where each row corresponds to a different reduction factor. When looking at the magnified images (see Figure 11b) it is clearly observed that the sidelobes reflections, detected in the middle of the left ventricle, is indeed locally weaker in magnitude compared with the speckle reflections in the surrounding. A logarithmic scale graph of CR and CNR as a function of the number of elements is presented in Figure 9.

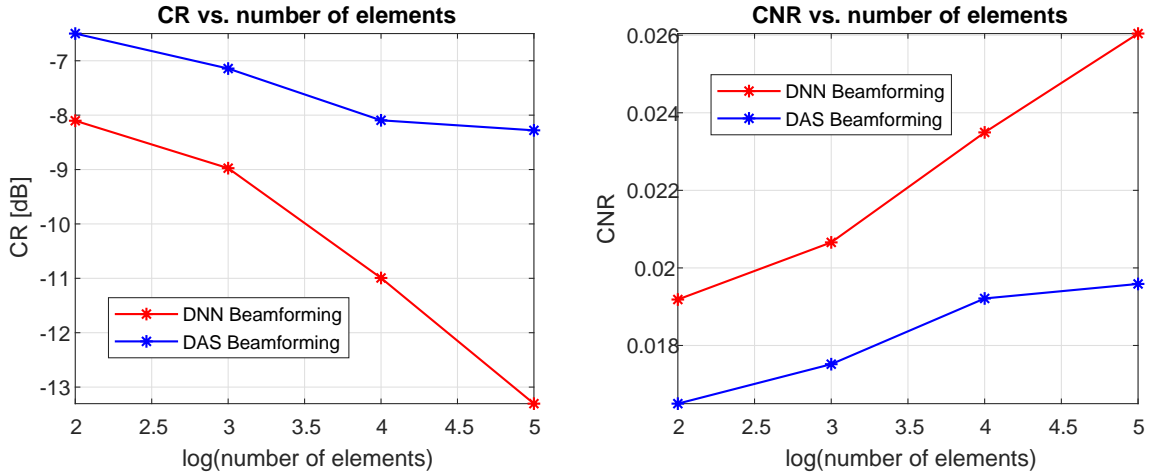


Fig. 9: Left: Contrast ratio vs. number of elements. Right: Contrast-to-noise ratio vs. number of elements.

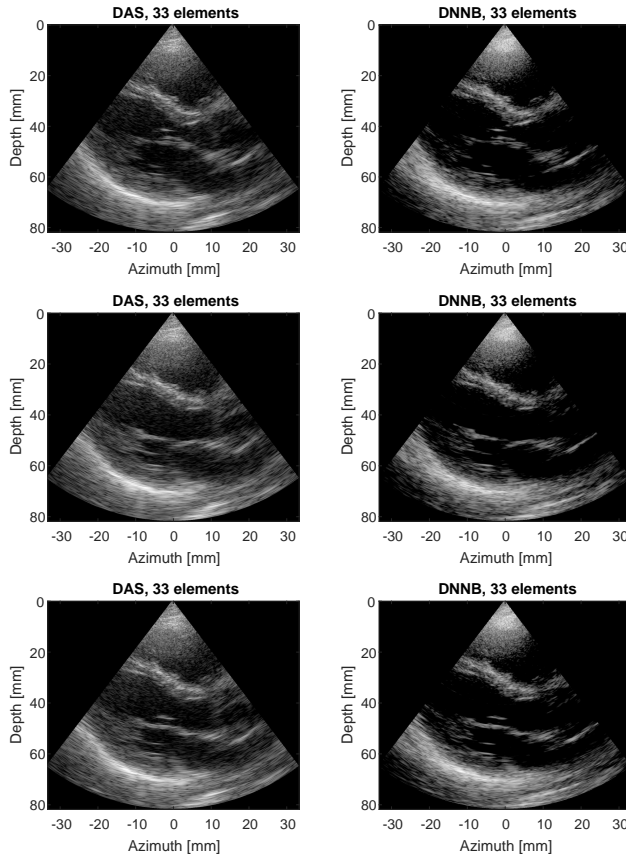


Fig. 10: Real Cardiac data results. The first column corresponds to DAS, and the second corresponds to the proposed method. Each row is corresponding to a different frame.

VI. CONCLUSION

In this paper, we proposed a deep learning-based method, DNNB, for the beamforming process in medical ultrasound. The network is trained to achieve two purposes: One, to emulate data from a larger array, and two, to suppress sidelobes.

By this, we managed to achieve both an improved resolution and improved contrast from a given array over the use of DAS on the available data. We demonstrate this both by simulation results and experiments on real cardiac data. The comparison shows the superior performance of DNNB in terms of both lateral resolution and contrast resolution. Our method shows the ability of sidelobe suppression using a neural network with fewer elements. The performance comparison between DAS 65 elements and DNNB 33 elements points to a trade-off between lateral resolution and contrast: the main improvement introduced by the proposed method is the significantly better contrast resolution. We note, however, that there is also better lateral resolution compared to DAS with the same number of elements. The reconstructed images obtained with the DNN beamformer achieve better CR and CNR due to significant suppression of the RMS sidelobe level compared to DAS. Accordingly, the reconstructed phantom cyst shows an improved edge definition, while preserving the speckle texture in the surrounding.

In conclusion, DNNB outperforms the DAS method when applied to the same data. Consequently, as pointed out earlier, fewer elements are required to reconstruct an image with high contrast and lateral resolution, paving the way to more efficient ultrasound devices.

REFERENCES

- [1] B. D. Van Veen and K. M. Buckley, "Beamforming: A versatile approach to spatial filtering," *IEEE assp magazine*, vol. 5, no. 2, pp. 4–24, 1988.
- [2] J. Cheng and J.-y. Lu, "Extended high-frame rate imaging method with limited-diffraction beams," *IEEE transactions on ultrasonics, ferroelectrics, and frequency control*, vol. 53, no. 5, pp. 880–899, 2006.
- [3] J. A. Jensen, S. I. Nikolov, K. L. Gammelmark, and M. H. Pedersen, "Synthetic aperture ultrasound imaging," *Ultrasonics*, vol. 44, pp. e5–e15, 2006.
- [4] R. Y. Chiao, L. J. Thomas, and S. D. Silverstein, "Sparse array imaging with spatially-encoded transmits," in *1997 IEEE Ultrasonics Symposium Proceedings. An International Symposium (Cat. No. 97CH36118)*, vol. 2. IEEE, 1997, pp. 1679–1682.
- [5] S. J. Norton, "Reconstruction of a reflectivity field from line integrals over circular paths," *The Journal of the Acoustical Society of America*, vol. 67, no. 3, pp. 853–863, 1980.
- [6] A. Lucas, M. Iliadis, R. Molina, and A. K. Katsaggelos, "Using deep neural networks for inverse problems in imaging: beyond analytical methods," *IEEE Signal Processing Magazine*, vol. 35, no. 1, pp. 20–36, 2018.

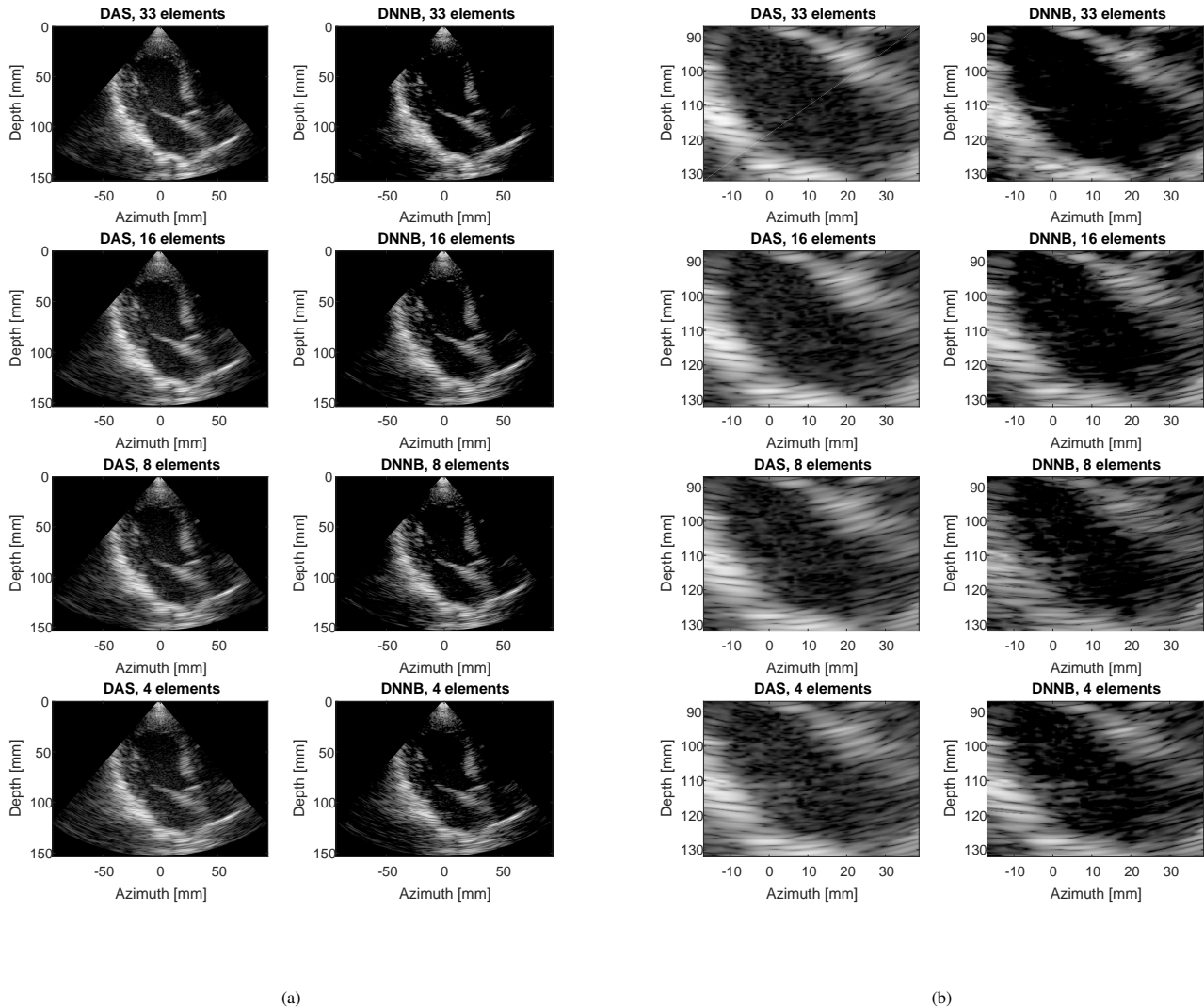


Fig. 11: (a) Real Cardiac data results. The first column corresponds to DAS, and the second corresponds to the proposed method. Each row is corresponding to a different reduction factor. (b) Zoom in of (a).

- [7] A. C. Luchies and B. C. Byram, "Deep neural networks for ultrasound beamforming," *IEEE transactions on medical imaging*, vol. 37, no. 9, pp. 2010–2021, 2018.
- [8] —, "Training improvements for ultrasound beamforming with deep neural networks," *Physics in medicine and biology*, 2019.
- [9] M. Gasse, F. Millioz, E. Roux, D. Garcia, H. Liebgott, and D. Friboulet, "High-quality plane wave compounding using convolutional neural networks," *IEEE transactions on ultrasonics, ferroelectrics, and frequency control*, vol. 64, no. 10, pp. 1637–1639, 2017.
- [10] A. A. Nair, M. R. Gubbi, T. D. Tran, A. Reiter, and M. A. L. Bell, "A fully convolutional neural network for beamforming ultrasound images," in *2018 IEEE International Ultrasonics Symposium (IUS)*. IEEE, 2018, pp. 1–4.
- [11] O. Senouf, S. Vedula, G. Zurakhov, A. Bronstein, M. Zibulevsky, O. Michailovich, D. Adam, and D. Blondheim, "High frame-rate cardiac ultrasound imaging with deep learning," in *International Conference on Medical Image Computing and Computer-Assisted Intervention*. Springer, 2018, pp. 126–134.
- [12] S. Vedula, O. Senouf, G. Zurakhov, A. Bronstein, M. Zibulevsky, O. Michailovich, D. Adam, and D. Gaitini, "High quality ultrasonic multi-line transmission through deep learning," in *International Workshop on Machine Learning for Medical Image Reconstruction*. Springer, 2018, pp. 147–155.
- [13] S. Vedula, O. Senouf, G. Zurakhov, A. Bronstein, O. Michailovich, and M. Zibulevsky, "Learning beamforming in ultrasound imaging," *arXiv preprint arXiv:1812.08043*, 2018.
- [14] W. Simson, M. Paschali, N. Navab, and G. Zahnd, "Deep learning beamforming for sub-sampled ultrasound data," in *2018 IEEE International Ultrasonics Symposium (IUS)*. IEEE, 2018, pp. 1–4.
- [15] B. Luijten, R. Cohen, F. J. de Bruijn, H. A. Schmeitz, M. Mischi, Y. C. Eldar, and R. J. van Sloun, "Deep learning for fast adaptive beamforming," in *ICASSP 2019-2019 IEEE International Conference on Acoustics, Speech and Signal Processing (ICASSP)*. IEEE, 2019, pp. 1333–1337.
- [16] D. Perdios, M. Vonlanthen, A. Besson, F. Martinez, M. Arditi, and J.-P. Thiran, "Deep convolutional neural network for ultrasound image enhancement," in *2018 IEEE International Ultrasonics Symposium (IUS)*. IEEE, 2018, pp. 1–4.
- [17] S. J. Norton, "Theory of acoustic imaging," *PhDT*, 1977.
- [18] C. Dong, C. C. Loy, K. He, and X. Tang, "Image super-resolution using deep convolutional networks," *IEEE transactions on pattern analysis and machine intelligence*, vol. 38, no. 2, pp. 295–307, 2015.
- [19] J. A. Jensen, "Field: A program for simulating ultrasound systems," in *10TH NORDICBALTIC CONFERENCE ON BIOMEDICAL IMAGING, VOL. 4, SUPPLEMENT 1, PART 1: 351–353*. Citeseer, 1996.
- [20] F. Chollet *et al.*, "Keras," <https://keras.io>, 2015.
- [21] M. Abadi *et al.*, "TensorFlow: Large-scale machine learning on heterogeneous systems," 2015, software available from tensorflow.org. [Online]. Available: <http://tensorflow.org/>

- [22] D. P. Kingma and J. Ba, "Adam: A method for stochastic optimization," *arXiv preprint arXiv:1412.6980*, 2014.
- [23] M. A. Lediju, G. E. Trahey, B. C. Byram, and J. J. Dahl, "Short-lag spatial coherence of backscattered echoes: Imaging characteristics," *IEEE transactions on ultrasonics, ferroelectrics, and frequency control*, vol. 58, no. 7, pp. 1377–1388, 2011.
- [24] O. M. H. Rindal, S. Aakhus, S. Holm, and A. Austeng, "Hypothesis of improved visualization of microstructures in the interventricular septum with ultrasound and adaptive beamforming," *Ultrasound in Medicine & Biology*, vol. 43, no. 10, pp. 2494–2499, 2017.

Nissim Peretz received the B.Sc. degree in electrical engineering from the Department of Electrical Engineering, Technion, Haifa, Israel, in 2015, where he is currently pursuing the M.Sc. degree in Electrical Engineering at the Technion.

Arie Feuer (M'76–SM'93–F'04–LF'14) has been with the Department of Electrical Engineering at the Technion - Israel Institute of Technology, since 1983 where he is currently a Professor Emeritus. He received his B.Sc. and M.Sc. from the Technion in 1967 and 1973 respectively and his Ph.D. from Yale University in 1978. From 1967 to 1970 he was in industry working on automation design and between 1978 and 1983 with Bell Labs in Holmdel, N.J. Between the years 2013 and 2015 he worked for a startup company developing algorithms for medical ultrasound imaging. Between the years 1994 and 2002 he served as the president of the Israel Association of Automatic Control and was a member of the IFAC Council during the years 2002-2005. Arie Feuer is a Life Fellow of the IEEE. In the last 25 years he has been regularly visiting the EECS department at the University of Newcastle. In 2009 he received an honorary doctorate from the University of Newcastle. His current research interests include medical imaging, in particular ultrasound and CT, resolution enhancement of digital images and videos, 3D video and multi-view data, sampling and combined representations of signals and images, and adaptive systems in signal processing and control.